Gaussian Distribution-Based Inertial Control of Wind Turbine Generators for Fast Frequency Response in Low Inertia Systems

Mostafa Kheshti, *Senior Member, IEEE*, Shuyue Lin, Xiaowei Zhao, Lei Ding, *Senior Member, IEEE*, Minghui Yin, *Member, IEEE*, Vladimir Terzija, *Fellow, IEEE*

***Abstract*— According to recent grid codes, large-scale wind turbines (WTs) are required to provide fast frequency response (FFR). The existing stepwise inertial control methods suggest immediate incremental power injection by WTs, followed by the abrupt over-production termination to avoid over-deceleration of the rotor speed. These methods have a drawback that they impose severe secondary frequency drops (SFD), or they consider an unrealistic constant wind speed during their inertial control support. This paper proposes a novel Gaussian distribution-based inertial control (GDBIC) scheme that can improve the frequency nadir without rotor speed over-deceleration. Upon detecting a power imbalance, WT increases the output power with an incremental power and declines it following Gaussian distribution trajectory controlled by a standard deviation parameter, ensuring by this convergence of the rotor speed to a stable equilibrium. The proposed scheme is also capable of responding to a second cascade event. The performance of the GDBIC is tested on the wind-integrated IEEE 9-bus system and the IEEE 39-bus system in DIgSILENT PowerFactory. It is also compared with other methods reported in literature. Furthermore, experimental tests are used to verify the performance of the proposed scheme, using two different hardware-in-the-loop testing facilities. The blade fatigue is studied using Fatigue, Aerodynamics, Structures, and Turbulence (FAST) Code. The simulation and experimental results showed that the release of the kinetic energy in rotors using the proposed GDBIC scheme allows significant improvement of the frequency nadir, with no SFD, as well as contribute to reliable operation during abrupt wind changes.**

Keywords—frequency control, Gaussian distribution, hardware-in-the-loop, stepwise inertial control, wind turbine

NOMENCLATURE

P_m	Mechanical power of wind turbine generator
ρ	Air density at the wind turbine blades
r	Radius of wind turbine blades in meter
C_p	Aerodynamic performance coefficient
λ	Tip-peed ratio of the wind turbine
β	Pitch angle of the wind turbine
v_w	Wind speed flowing to the blades in m/s
ω_r	Instantaneous rotor speed of wind turbine
P_{MPPT}	Maximum power point tracking power output of wind turbine
P_0	Active power output of wind turbine
k_{opt}	Coefficient of maximum power point tracking curve
ΔP_f	Wind turbine incremental power at over-production
x_0	Mean value of a Gaussian distribution function
σ	Standard deviation of the Gaussian distribution function
a	Height of a Gaussian distribution function
ω_0	Rotor speed working point prior to a disturbance
ω_{min}	Minimum rotor speed limit of a wind turbine
ω_{off}	Rotor speed at the over-production termination
ω_{mean}	The average rotor speed between the minimum and the working point
f_{nadir}	The frequency nadir
RES	Renewable energy sources
FFR	Fast frequency response
WT	Wind turbine
SIC	Stepwise inertial control
SFD	Secondary frequency drop
MPPT	Maximum power point tracking
ROCOF	Rate of change of frequency
DFIG	Doubly fed induction generator
AGC	Automatic generation control
TOP	Temporary over-production
GDBIC	Gaussian distribution-based inertial control
HIL	Hardware-in-the-loop
RMS	Root means square
FAST	Fatigue, Aerodynamics, Structures, and Turbulence
NREL	National Renewable Energy Laboratory

This work was supported by the U.K. Engineering and Physical Sciences Research Council under Grant EP/S000747/1.

M. Kheshti and X. Zhao (Corresponding Author) are with the Intelligent Control and Smart Energy (ICSE) Research Group, School of Engineering, University of Warwick, Coventry CV4 7AL, U.K. (e-mails: mostafa.kheshti@warwick.ac.uk; xiaowei.zhao@warwick.ac.uk).
S. Lin is with the Department of Engineering, the University of Hull, Hull, HU6 7RX, UK (email: s.lin@hull.ac.uk)
L. Ding is with the Key Laboratory of Power System Intelligent Dispatch and Control, Shandong University, Jinan, China (email: dinglei@sdu.edu.cn)
M. Yin is with the School of Automation, Nanjing University of Science and Technology, Nanjing 210094, China (e-mail: ymhui@vip.163.com).
V. Terzija is with the Center for Energy Science and Technology, Skolkovo Institute of Science and Technology, Moscow, Russia (v.terzija@skoltech.ru).

I. INTRODUCTION

With the increasing shares of power-electronic interfaced variable renewable energy sources (RESs), the frequency

changes in low inertia power systems become more volatile and unpredictable. Large frequency deviations could jeopardize the grid frequency stability and cause outages and even catastrophic blackouts [1].

Transmission system operators have stipulated new grid codes, enforcing wind farms to contribute to the grid frequency support [2], [3]. However, the way how a variable speed wind turbine (WT) could participate in frequency control, in form of the inertial control is a task that engineers and researchers in industry and academia are tackling since 2004 [4], [5].

In essence, a WT operates at the maximum power point tracking (MPPT) to generate maximum electric power. To contribute to the fast frequency response (FFR), WTs need to switch away from the MPPT, enter the stage of over-production and the consequent rotor speed recovery process [6], [7]. The literature focuses on the frequency nadir (f_{nadir}) improvement, which are divided into two general types: a) frequency-based inertial control and b) stepwise inertial control (SIC) schemes.

Frequency-based inertial control schemes add additional control loops based on the measured frequency [8], [9], the rate of change of frequency (ROCOF) [10], [11] and the ROCOF and droop [12], [13]. Frequency-based inertial control contributes to the improvement of frequency nadir; however, these loops contain relatively slow response and less frequency support contribution, due to the continuous measurement of frequency and ROCOF. Also, they contain gain tuning in the frequency control loop and the low and high pass filters. Poor parameter tuning could lead to a worsen grid frequency nadir compared to uncommitted WTs' operation. The ROCOF signal as the input to these controllers may introduce some noise in frequency derivative measurement [14].

The SIC methods intend to enhance the frequency support effect of WTs with the implementation that is independent on frequency measurements [15-17]. Intuitively, the SIC is characterized with a fast response to frequency decline [18]. Upon detecting an event, SIC quickly increases the WT active power output and remains in the over-production state for a predefined time [19-20]. SIC can improve the frequency nadir more than frequency-based inertial schemes [21]. However, in SIC schemes, to ensure that the rotor speed does not over-decelerate, the over-production abruptly terminates to allow rotor speed recovery, causing a secondary disturbance [22], [23]. In [19], an intelligent neural network-based approach was proposed to identify the adequate utilization of kinetic energy for the FFR. This method requires updates in its framework in presence of system topology changes. In [20] a time-domain power reference scheme is proposed with 10s overproduction time and a 20s rotor speed recovery. However, a power drop with the magnitude of 1.5 times the incremental power at the termination of this scheme causes a serious secondary frequency drop (SFD). In [23], to mitigate the SFD, the rotor recovery follows an underproduction path along the mechanical power curve of the rotor. But this approach suffers from excessive extraction of the kinetic energy, and longtime recovery regardless of the size of disturbance or the wind variation. In [24], a coordination scheme between the WTs and the energy storage system was used to improve the frequency nadir, while the SFD was still notable. In [25] and [26], the WT output power is optimized during the inertia response to reduce the SFD.

The main challenges for the existing SIC methods in literature are that the wind speed has been considered constant during their operation. The FFR capability for a second cascade event has not been considered. Furthermore, these methods impose a SFD to the grid that in some cases, it could be worse than the first frequency nadir or the cases without WT's participation. Results presented in [27] and [28] showed that the higher penetration level of the wind energy will cause larger SFD. Therefore, it is vital to develop a robust control scheme with FFR capability to improve the frequency nadir against dynamical changes.

Motivated to overcome the deficiencies of SIC methods, this paper proposes a novel Gaussian distribution-based inertial control (GDBIC) scheme that naturally contributes to the frequency support upon detecting a power imbalance. An incremental power is injected and the WT will immediately follow a pre-defined formulated Gaussian trajectory to reach a designated equilibrium working point, ensuring stable operation of the WT rotor. The main novelties and contributions of the paper are as follows.

- A novel GDBIC scheme is proposed to use an adequate portion of available kinetic energy in the WT rotating mass during FFR. A standard deviation term σ is formulated as control parameter for the participation of WTs in different wind speed conditions, without imposing SFD.
- During the FFR, the rotor converges to an equilibrium working point where the WT rotor speed is the mean value between the MPPT operation and the minimum rotor speed limit. It remains at this equilibrium point until the Automatic Generation Control (AGC) is activated or a cascade event is identified.
- For the first time, this paper also considers a cascade event. In such case, the scheme can launch another FFR using the remaining available stored kinetic energy in the rotating mass using a new σ.
- The proposed control scheme is tested and validated on the Western System Coordinating Council 9-bus test system and the IEEE 39-bus, New-England Power System as well as two different experimental platforms. The results are compared with other existing methods, namely, inertial control [20], modified SIC [22], temporary over-production (TOP) scheme [23], linear inertial control [18], and the MPPT operation of the wind farm. The comparison demonstrates the effectiveness of the proposed method for wind farm frequency control and provides important conclusions.
- To evaluate the effects of the proposed method on the blade fatigue, the root loads and tip motions of blade are compared by applying the NREL's FAST code on the wind turbine simulator. The results show that when applying the proposed GDBIC, the improvement of frequency nadir is not at the cost of blade fatigue.

The rest of this paper is organized as follows: Section II presents the WT and the state-of-the-art SIC schemes. The proposed GDBIC and its FFR capability is explained in section III. Section IV contains the simulation results on IEEE 9-bus and IEEE 39-bus systems using DIgSILENT PowerFactory as well as the experimental validations using two different hardware-in-the-loop (HIL) test rigs. Section V concludes this paper.

II. Wind Turbine Inertial Control

The mechanical power of WTs is a cubic function of wind speed, which is formulated as:

$$P_m = \frac{1}{2}\rho\pi r^2 C_p(\lambda,\beta)v_w^3 \quad (1)$$

where ρ is the air density; r is the radius of WT blades; the wind speed hitting the WTs blades is shown as v_w. The aerodynamic performance C_p in which depends on the tip-peed ratio λ and the pitch angle β, is presented based on the following form [19]:

$$C_p(\lambda,\beta) = 0.22\left(\frac{116}{\lambda_i} - 0.4\beta - 5\right)e^{\frac{-12.5}{\lambda_i}} \quad (2)$$

$$\lambda_i = \left(\frac{1}{\lambda + 0.08\beta} - \frac{0.035}{\beta^3 + 1}\right)^{-1} \quad (3)$$

$$\lambda = \frac{r\omega_r}{v_w} \quad (4)$$

where ω_r is the WT rotor speed. The maximum aerodynamic performance $C_p(\lambda,\beta)$ of WT appears when β=0, shown in Fig. 1.

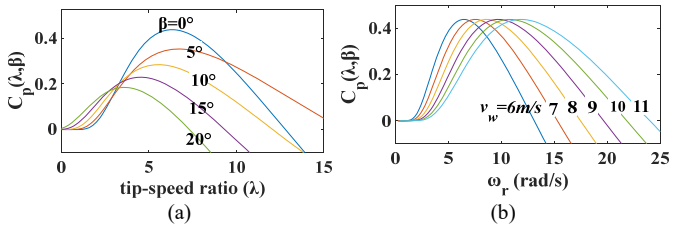

Fig. 1. Aerodynamic performance of a WT (a) as a function of λ and β (b) as a function of v_w, and ω_r when β=0.

During normal operation, WTs operate at the MPPT mode to generate maximum electric output power:

$$P_{MPPT}(\omega_r) = k_{opt}\omega_r^3 \quad (5)$$

where k_{opt} is the coefficient of MPPT curve of the turbine. To allow participation of WTs in FFR, they should switch away from the MPPT considering the mechanical limitations, i.e., the rotor speed limits and torque limits imposed on the turbine. In this paper, a new reference power scheme is proposed. It ensures safe operation of WTs within these limits and with higher frequency support compared to solutions proposed in the open literature.

In low inertia systems, severe frequency deviations can happen after abrupt disconnections of large generators or connections of big loads. The entire inertial frequency control must respond within few seconds, otherwise sharp rate of change of frequency may trigger under frequency load shedding, or even cause cascade outages and blackouts [33]. In a power system where synchronous generators are dominant, the release of kinetic energy from the rotating masses of the synchronous generators and induction machines happens autonomously. In variable RES dominated power systems, these decoupled energy resources emulate the natural inertia provision of synchronous generators to ensure secure system response to large active power imbalances.

To arrest frequency excursions, WTs can contribute to frequency control support. To do that, several schemes have been proposed by researchers in the past [29]. Some of the main schemes are briefly explained, as shown in Fig. 2. Then, our proposed inertial control method is formulated, to overcome the deficiencies of the existing methods. The proposed method provides a safe operation of WTs, and better grid frequency support compared with the quoted existing methods in literature. We will develop and apply these methods and investigate their frequency arrest performances on the same case study systems.

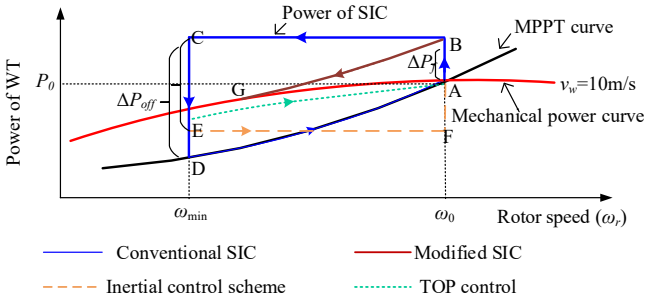

Fig. 2. Stepwise inertial control schemes

A. *Inertial control* [20]

In this time domain scheme, shown by the trajectory ABCEFA in Fig. 3, prior to any disturbance, a WT operates with power output P_0 and the rotor speed ω_0 on the MPPT curve shown as point A.

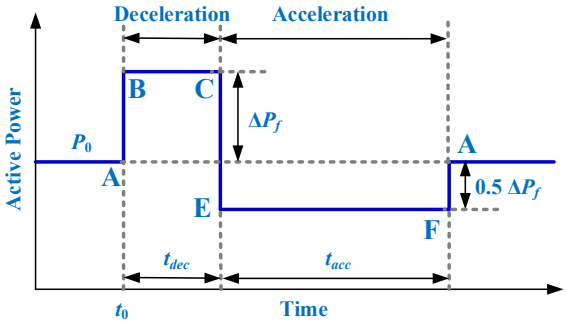

Fig. 3. Time domain inertial control scheme.

When a frequency event occurs, the WT injects an incremental power, moving from point A to B and operates in over-production for a period of 10 seconds, suggested by the authors to address the Hydro-Québec requirement. During this over-production stage, the mismatch between higher electrical power and lower mechanical power imposes decline in the rotor speed. To avoid the rotor stall, the output power then immediately falls from point C with magnitude of P_0 +ΔP_f to point E, with the magnitude of P_0 -0.5ΔP_f and remains at this

power level until the rotor speed is recovered back to its nominal value.

This time-domain method is unable to reliably operate in practice for different wind conditions. The large power drop at C to E with magnitude of $1.5\Delta P_f$ imposes an undesirable large SFD to the grid. For the wind speeds bigger than 7.5 m/s, the incremental power is 0.1 p.u., while for wind speeds smaller than or equal to 7.5 m/s, the incremental power is 0.05 p.u, which limits the contribution of this scheme. Also, the small incremental power gain in this method is inevitable, limiting its FFR contribution.

B. *Modified SIC* [22]

In this scheme, shown by the ABG route in Fig. 4, once a power disturbance occurs, the wind turbine injects incremental power ΔP_f and immediately starts declining parallel with the MPPT curve. Here the rotor speed decreases and converges to a new equilibrium point, ω_{off}. However, to ensure rotor speed convergence, the incremental power cannot be a large value, which affects the efficacy of the scheme. In this regard, the shaded region in the over-production period is equal to the shaded region below the mechanical power, formulated as follows:

$$\int_{\omega_{min}}^{\omega_{off}} \left(P_m - P_{MPPT} - \Delta P_f \right) d\omega = 0 \tag{6}$$

$$\Delta P_f = \frac{1}{\omega_{off} - \omega_{min}} \left(\int_{\omega_{min}}^{\omega_{off}} P_m \, d\omega - \int_{\omega_{min}}^{\omega_{off}} P_{MPPT} \, d\omega \right) \tag{7}$$

Also, at the instance of rotor deceleration stage, the dP_{ref}/dt could be large, what can cause a late, but significant, frequency nadir.

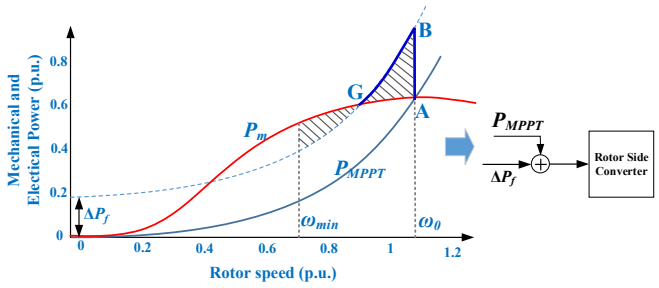

Fig. 4. Modified stepwise inertial control scheme.

C. *Temporary Over-Production (TOP)* [23]

The TOP scheme is drawn as the ABCEA route in Fig. 2, and it is illustrated in the time domain in Fig. 5. When a large frequency drop occurs, the WT operates in the over-production by injecting an incremental power. The WT then remains in over-production with output power of $P_0 + \Delta P_f$. Once the rotor speed reaches to the 0.7 p.u. for DFIGs, the reference output power drops slightly lower than the mechanical power curve, so that the rotor speed can be recovered.

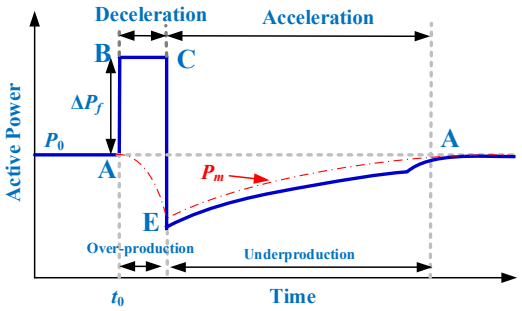

Fig. 5. Time domain characteristics of the TOP scheme.

However, at this scheme, excessive amount of kinetic energy is extracted regardless of magnitude of disturbance or the wind speed. As the rotor speed reaches to the lower boundary of 0.7 p.u., slight noise, uncertainties or measurement errors could cause rotor stalls. Besides, long rotor speed recovery jeopardizes the entire frequency support if abrupt changes in wind speed occurs, causing worsen SFD.

III. Proposed GDBIC Scheme

A. *GDBIC scheme concept*

The main objective of the WT fast frequency control is to improve the grid frequency nadir, caused by the abrupt trip of large generators or connection of big loads to the system. However, most of the existing schemes consider WT rotor recovery, immediately after contributing to the frequency mitigation. As the power system is still in its transient state of frequency control, WT rotor speed recovery operation may be at cost of jeopardizing the entire frequency control. For example, a sudden decrease of wind speed, or abrupt termination of inertial control in these methods, will impose a severe SFD. The existing methods also assume that the wind speed remains constant during the entire FFR process. Such an unrealistic assumption is different from the practical scenarios. Moreover, these methods have not considered cascade events, where a second disturbance may occur in the grid, during inertial control operation of WTs.

Therefore, a novel inertial control scheme is proposed to operate reliably in presence of changes of the wind speed, or when a second external active power disturbance occurs in the grid, during the FFR operation. The proposed scheme will improve the grid frequency nadir and support reaching a stable equilibrium point, terminating the service and remains in the equilibrium point until the grid frequency is settled. The settling frequency using the proposed GDBIC will allow the AGC to be later activated and to eliminate the steady state error. Also, if the wind speed changes or a cascade event occurs during the frequency support, the proposed scheme is able to operate robustly and provide frequency nadir improvement.

Gaussian distribution is an archetypal bell curve shape function which is frequently appeared in nature and represented in a general form as follows:

$$f(x) = a e^{-\frac{(x-x_0)^2}{2\sigma^2}} \tag{8}$$

where a is the height of the Gaussian curve, x_0 is the mean value in which the values of x are symmetrically distributed around it with standard deviation of σ. The value of σ shows how quickly or slowly the distribution happens.

In this paper, we use the concept of Gaussian distribution in WT inertial control and utilize the concept of standard deviation σ as a control parameter. The stages of the proposed inertial control scheme are shown in Fig. 6 (a) and described as follows:

A-B: Prior to the disturbance, WT is operating at the MPPT mode with the nominal rotor speed (ω_0) and electric power output P_0. Upon observing a power imbalance in the grid, its output power increases with the incremental value of ΔP_f, which is equivalent to the height of the Gaussian curve.

B-C: As the electrical power of the WT is bigger than the mechanical power, the rotor speed decelerates. WT gradually decreases its over-production following an optimum Gaussian distribution trajectory controlled by the standard deviation σ. The rotor speed declines to ω_{off} which must be larger than the speed limit of 0.7 p.u. in DFIG WTs.

C-A: The WT is at the equilibrium point where the electrical and mechanical power are equal. The gap between point C and A is compensated by the secondary frequency control assigned by the system operator, in which the WT is eventually back to the MPPT mode. This allows an autonomous operation of WTs for FFR and in coordination with the AGC, without unnecessary risky operation of the WTs during frequency arrest.

In a case of unexpected cascade event during the inertial control response, the trajectory B-C is shifted to another Gaussian trajectory where the new settling point (C) will be the midpoint between the minimum rotor speed limit and the current rotor speed upon detecting the second cascade event. This new trajectory will inject further kinetic energy into the grid in form of active power to mitigate the consequent frequency deviation caused by the unexpected cascade event. The new settling point of the rotor ensures safe operation of the WT without over-deceleration. This mechanism in form of a reference power is sent to the rotor side converter, as shown in Fig. 6 (b).

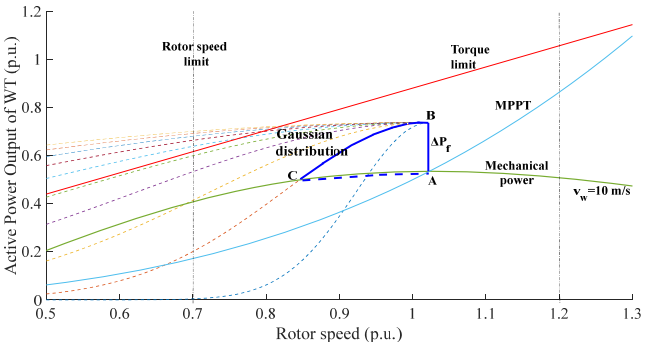

(a)

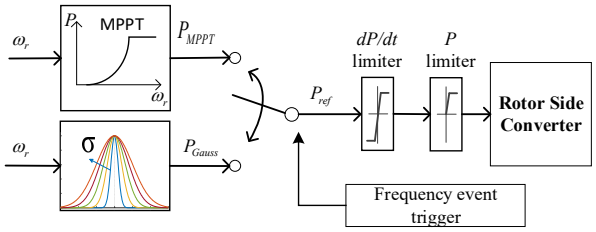

(b)

Fig. 6. Proposed GDBIC in a DFIG WT (a) power−rotor speed plane (b) control block.

B. GDBIC scheme formulation

The GDBIC during the over-production stage is formulated as follows:

$$P_{Gauss}(\omega_r) = \left(P_0 + \Delta P_f\right) e^{-\frac{(\omega_r - \omega_0)^2}{2\sigma^2}} \tag{9}$$

In this proposed scheme, two questions arise, i) how much incremental power a WT should support for frequency control? and ii) which trajectory should the WT select in the deceleration stage?

The first question is carefully assessed based on intensive simulations and experimental verifications. The incremental power with one-third to half of the power imbalance can significantly contribute to the grid frequency nadir improvement [18], [19]. The second question can be formulated as the question of which value of σ should be set, which is tackled in this paper.

When the WT operates at the over-production stage, the rotor speed declines which must be kept bigger than the rotor stall limit. Also, the over-produced power should be able to notably improve the frequency nadir. Considering these factors, the proposed scheme considers that the Gaussian distribution curve intersects with the mechanical power curve at a specific rotor speed called ω_{off}. At this point both mechanical power in (1) and the Gaussian distribution in (9) are equal:

$$P_m(\omega_{mean}) = P_{Gauss}(\omega_{mean}) \tag{10}$$

where ω_{mean} is the average rotor speed between the nominal working rotor speed and the minimum allowable speed of 0.7 p.u.

$$\omega_{mean} = \frac{\omega_0 + \omega_{\min}}{2} \tag{11}$$

By calculating the mechanical and Gaussian distribution power at the point ω_{mean}, the desired value of σ can be obtained:

$$P_{Gauss}(\omega_{mean}) = \left(P_0 + \Delta P_f\right) e^{-\frac{(\omega_{mean}-\omega_0)^2}{2\sigma^2}}$$

$$e^{-\frac{(\omega_{mean}-\omega_0)^2}{2\sigma^2}} = \frac{P_{Gauss}(\omega_{mean})}{\left(P_0 + \Delta P_f\right)} \xrightarrow{P_{Gauss}(\omega_{mean}) = P_m(\omega_{mean})}$$

$$-\frac{(\omega_{mean}-\omega_0)^2}{2\sigma^2} = \ln \frac{P_{m,\,\omega_{mean}}}{\left(P_0 + \Delta P_f\right)} \tag{12}$$

$$\sigma = \sqrt{-\frac{(\omega_{mean}-\omega_0)^2}{2\ln \dfrac{P_{m,\,\omega_{mean}}}{\left(P_0 + \Delta P_f\right)}}}$$

where

$$p_{m,\,\omega_{mean}} = 0.11\left(\frac{116}{\lambda_i} - 0.4\beta - 5\right)\rho\pi r^2 v_w^3 e^{\frac{-125}{\lambda_i}} \tag{13}$$

$$\lambda_i = \left(\frac{v_w}{r\omega_{mean} + 0.08\beta v_w} - \frac{0.035}{\beta^3 + 1}\right)^{-1} \tag{14}$$

The obtained value of σ in (12) shows which Gaussian distribution trajectory should be taken by the WT for better grid frequency support. The proposed GDBIC of WTs with the control parameter of σ is shown in Fig. 7. The convex form of the Gaussian function with downward concavity will ensure that there is an intersection with the mechanical power curve. Also, the average rotor speed ω_{mean} in (11) is the intersection point which is an equilibrium point that ensures safe operation of the WT, adequate portion of kinetic energy reserve for the extreme contingencies, as well as providing a settling frequency that will activate the AGC.

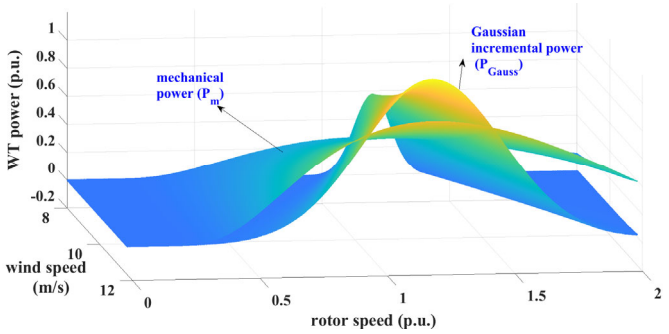

Fig. 7. Convergence of the proposed GDBIC to the equilibrium points on mechanical power using σ.

In the proposed scheme and as shown in Fig. 7, σ is larger when wind speed is higher, while it is smaller for slower wind speeds. In other words, the proposed scheme ensures safe operation of the WT under intermittent wind condition within the operating limits. The standard deviation σ is obtained for different wind speeds, which can be conveniently implemented by the WT controller and manufacturers.

IV. Simulation and Experimental Results

To investigate the applicability of the proposed scheme, two standard test systems are used, namely IEEE 9-bus system and the IEEE 39-bus system. Also, the proposed scheme is validated using two different state-of-the-art experimental platforms. The results are compared with other existing methods known from the open literature, e.g., inertial control method [20], modified SIC [22], TOP method [23], linear inertial control [18], and the MPPT operation of the wind farm. These methods have been properly developed and tuned based on their corresponding references and the tests are conducted on the same test system and network parameters for the sake of fair comparisons.

A. Simulation Validations-IEEE 9-bus test system

The proposed GDBIC is tested using the modified IEEE 9-bus system in DIgSILENT PowerFactory. As illustrated in Fig. 8, a large-scale 100 MW DFIG wind farm is integrated into the system. Details of the model and the parameters are available in [19]. The proposed scheme is tested against different sizes of power imbalances and wind speeds.

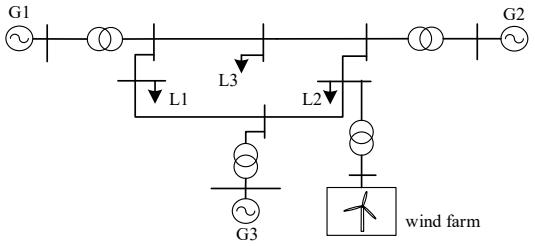

Fig. 8. Case study of the 100 MW wind integrated IEEE-9 bus system.

The performance of the proposed scheme is verified in presence of different wind speeds in the wind farm. It is assumed that a large active power imbalance of 35% occurs by sudden increase of load L3 at time t=0.

Upon occurrence of the large power imbalance, the WTs operation was switched from the MPPT to the incremental power injection followed by a designated Gaussian distribution, as shown in Fig. 9. Small difference between the final electric power of the WT and the MPPT mode operation is advantageous.

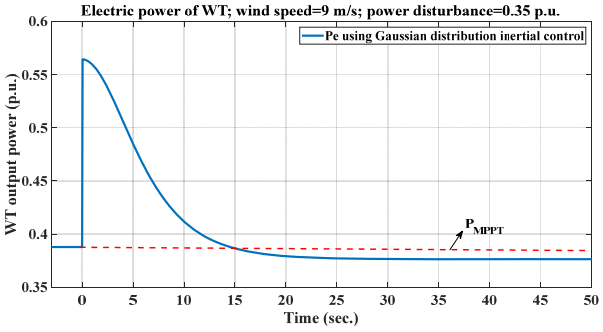

Fig. 9. Electric output power of WTs using the proposed inertial control scheme.

The grid frequency nadir by different methods are shown in Fig. 10, which verifies that frequency support contribution of the proposed scheme provides a much better improvement of frequency nadir. Also, this scheme does not impose a SFD to the grid, while other methods impose severe frequency excursions. Based on the comparisons, the proposed scheme

extracts an adequate portion of available kinetic energy from the rotating mass of WT, while excessive exploitation by other methods have resulted in dipper nadirs and unsafe SFDs. The difference between the frequency nadir improvement of the proposed scheme and the MPPT mode which the WTs do not contribute to frequency control, is notable.

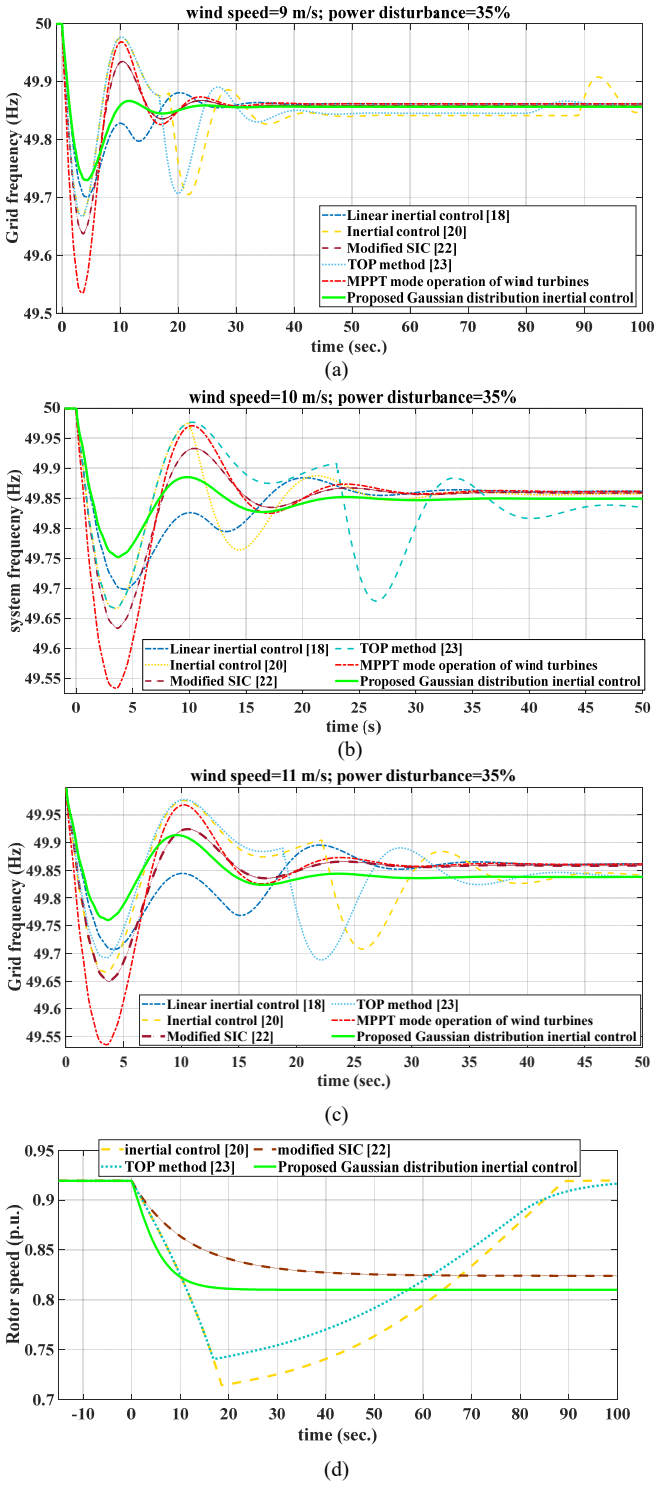

Fig. 10. Improvement of the grid frequency nadir with the proposed GDBIC under different wind speeds (a) v_w=9m/s (b) v_w=10m/s (c) v_w=11m/s (d) rotor speed convergence to their equilibrium points.

Fig. 10 (d) shows the convergence of rotor speed to the ω_{mean}. It can be seen that the WT rotor speed using the proposed scheme, converges faster to a new equilibrium point compared with other methods, which ensures safe and stable operation of the WT for any wind speed within the speed limits operation.

In literature, the inertial control schemes consider the wind speed as a constant parameter in an unrealistic time window of tens of seconds to minutes. Such an assumption may result in unfeasibility of practical applications. To simulate a realistic scenario, it is assumed that a power disturbance of 35% occurs at t=100s, and the wind speed suddenly drops from 9m/s to 8m/s at t=105s. Performance of the proposed GDBIC is verified against the frequency event and this abrupt wind speed change, as shown in Fig. 11. It is seen that two main frequency nadirs are formed. The first frequency nadir is due to the power disturbance while the SFD is due to the wind speed change. Other inertial control methods impose severe dipper frequency nadirs which may even result in outages in practice. However, the proposed scheme has a reliable performance against wind speed intermittency. That is because the concavity of the scheme is downward and the equilibrium intersection of the GDBIC and the mechanical power is designed to be around the average rotor speed, as formulated in (12).

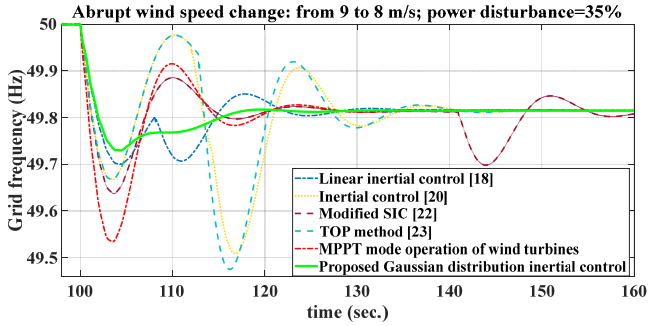

Fig. 11. Reliable performance of the proposed GDBIC against wind speed change.

As formulated in (11), we suggest that the new equilibrium point or the settling rotor speed of WTs be set as ω_{mean}. That is because if the corresponding σ is selected as too small, the WT power reference will converge near the nominal working point of the turbine, contributing less in frequency nadir improvement, but with slightly better frequency settlement. If σ is selected too large, excessive kinetic energy is drained from the rotating blades, causing slight improvement in the frequency nadir, compared with ω_{mean}, but with smaller frequency settlement. In the case of continental Europe, the maximum steady state frequency deviation is 0.2 Hz in which if the settling frequency is lower than 200 mHz, the AGC will not activate to bring the frequency back to its nominal value. This effect is shown in Fig. 12. As it can be seen, by choosing ω_{mean} as the settling rotor speed, it gives a desired tradeoff with both acceptable frequency nadir and settling frequency value. This ensures a reliable and coordinated operation of WTs during FFR, and AGC to be enabled during the secondary frequency

response.

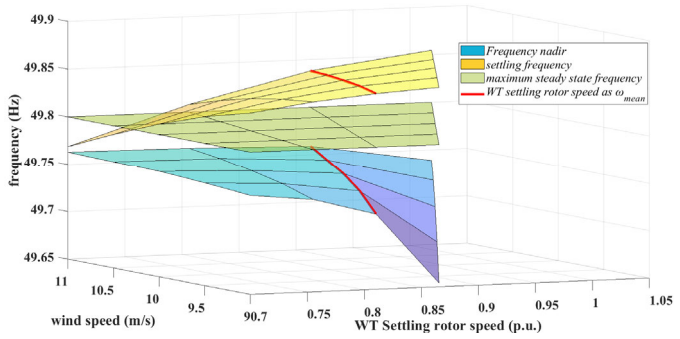

Fig. 12. Choosing ω_{mean} as the settling rotor speed with desired tradeoff between the grid frequency nadir and the settling frequency.

A scenario is also included in which the wind farm is considered as a non-aggregated model comprising 20 individual WTs. A large 0.35 p.u. disturbance occurs at t=100s. The wind farm operates under a stochastic wind profile at the time of disturbance, illustrated in Fig. 13(a). Each WT individually participates in the FFR with a corresponding GDBIC scheme governed by the control parameter σ, as presented in Table I. The imposed frequency effect caused by each WT is shown in Fig. 13(b). It can be seen that the grid frequency using the proposed method has a significantly safer and better frequency movement than the MPPT mode.

Table I GDBIC participation of each individual WT under a stochastic wind profile

WT No.	v_ω (m/s)	σ	WT No.	v_ω (m/s)	σ
1	9.4	0.1509	11	10.3	0.2182
2	9.9	0.1878	12	10.9	0.2645
3	10.2	0.2106	13	9.8	0.1804
4	11	0.2722	14	10.1	0.2030
5	10.8	0.2567	15	10.6	0.2413
6	9.6	0.1655	16	9.3	0.1437
7	9.5	0.1582	17	10.5	0.2336
8	10.7	0.2490	18	9.2	0.1366
9	9.7	0.1729	19	10	0.1954
10	9.1	0.1296	20	10.4	0.2258

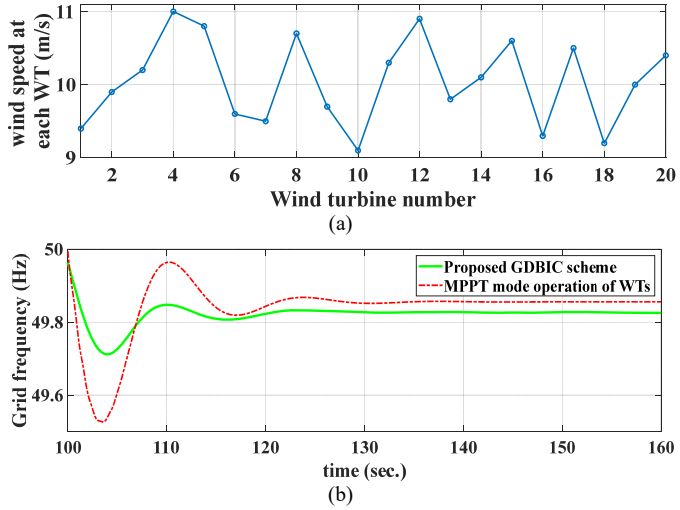

Fig. 13. Frequency control performance of the non-aggregated model of wind farm (a) Wind speed at each WT prior to the power imbalance (b) Grid frequency control with and without GDBIC scheme.

B. Simulation Validations-IEEE 39-bus system

The proposed scheme is also tested using the IEEE 39-bus test system, comprising 39 buses, 32 transmission lines, 24 transformers, 10 synchronous generators and one wind farm. The loads in the system consume 6373 MW and 1408 MVAr. Fig. 14 (a) shows this case study system. Except for generator G1, all other synchronous generators are equipped with the IEEE standard governor model shown in Fig. 14(b). The wind farm includes three clusters of 5 MW DFIG WTs, with the farm total capacity of 1500 MW. Parameters of the WTs are shown in Table A.1 in the Appendix. A sudden power disturbance event of 500 MW occurred in the system and performance of the proposed GDBIC and other existing methods are investigated.

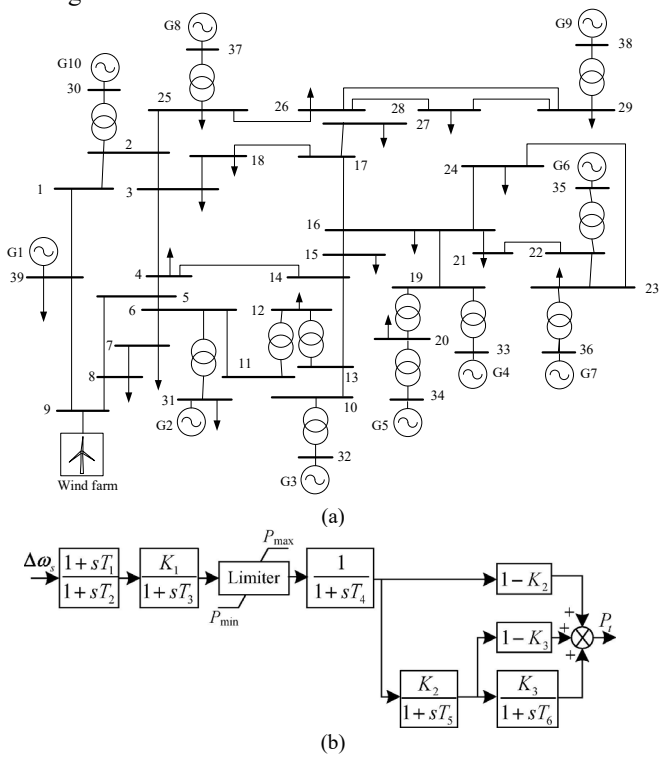

Fig. 14. Second Case study system (a) 1500 MW wind integrated IEEE-39 bus system (b) IEEE standard governor of the generators at IEEE 39-bus system.

The grid frequency results using different methods are shown in Fig. 15. Results obtained confirm that the frequency nadir is less critical in the case of the proposed GDBIC approach, utilizing less kinetic energy from the rotating blades and within the operating range of the machine.

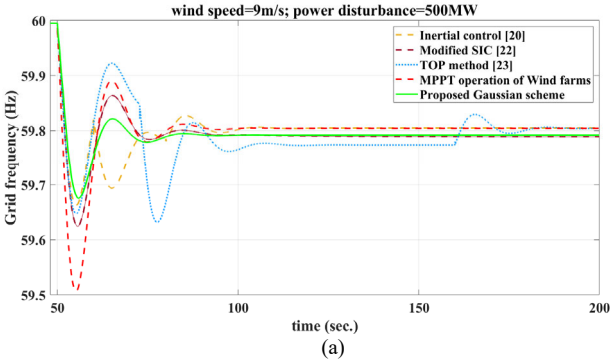

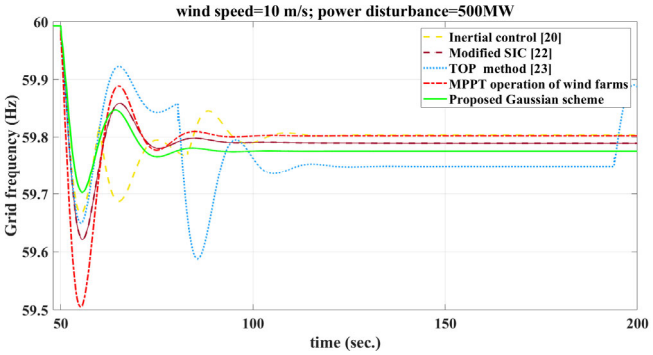

(b)

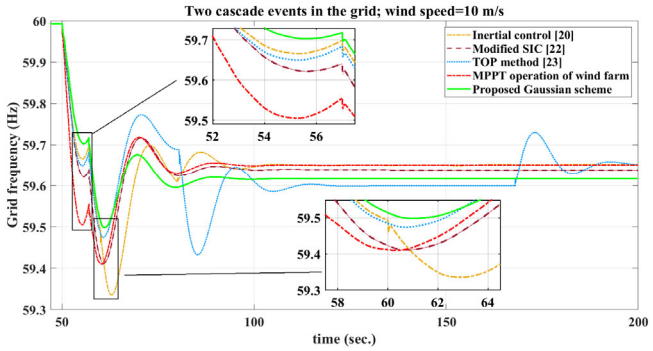

(c)

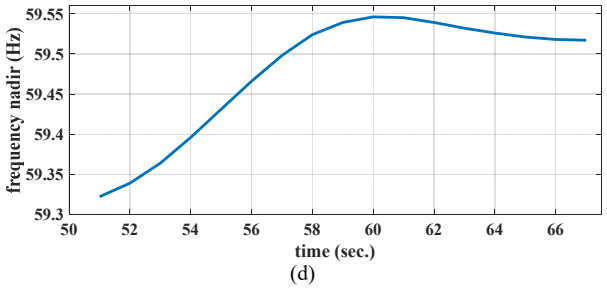

(d)

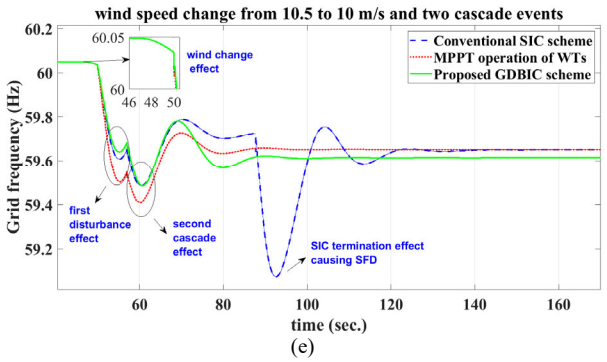

(e)

Fig. 15. Performance of different FFR schemes on grid frequency control in wind integrated IEEE 39-bus test system under (a) v_w=9m/s (b) v_w=10m/s (c) v_w=10m/s and two cascade events (d) impact of the timing of second event on the frequency nadir (e) wind speed change and two consecutive cascade events.

To investigate the performance of the quoted SIC schemes in a more severe scenario, it is assumed that two consecutive load events occur. Firstly, a 500MW load event occurs at bus 4, at t=50s. The second abrupt active power disturbance occurs randomly at a random time. Fig. 15 (c) shows the results of grid frequency control schemes against two cascade events where the second event appeared at the bus 39 with the size of 387 MW at t=57s. In the presence of the second event, the grid frequency using the inertial control scheme [20] and modified SIC [22] became worse than the case where WTs do not participate in grid frequency control. The consequent SFD of TOP scheme [23] has a severe nadir of 59.432Hz. On the contrary, the proposed GDBIC has improved the grid frequency nadirs during both cascade events. The first nadir is 59.7 Hz and the second nadir due to the load event is 59.5 Hz. As in reality, the second cascade event could occur at any instance randomly after the first event, Fig. 15(d) shows that when the second cascade event occurs early after the first event, the overall frequency nadir will be dipper. When the second event occurs at t=60s, the overall frequency nadir improvement is at the highest value. This is due to the overshoot of mechanical power of synchronous generators that coincided at the same time with the second cascade event.

Fig. 15 (e) shows the scenario where the wind speed at the wind farm drops from 10.5 m/s to 10 m/s at t=47s. Then, a 500 MW load event occurs in the grid at bus 4 at time t=50s. Afterwards, a second consecutive event of 387 MW occurs at bus 39 at time t=57s. The wind drop causes a slight change in the frequency as the WTs are operating at the MPPT mode prior to the first event. When the first event occurs, the frequency drops and the inertial control schemes are activated. The FFR and primary frequency control contain the frequency, in which the first frequency nadir appears. The second event causes a severe drop in the frequency. The conventional SIC schemes require to terminate their inertial control to avoid over-deceleration of the rotor. This action causes a drastic SFD that could trigger under-frequency load shedding and outages. The proposed GDBIC has performed reliably in presence of wind change and cascade events.

C. Experimental Validations 1

To validate the applicability and efficacy of the proposed GDBIC, experimental tests are conducted. Fig. 16 shows the single-bus power system experimental platform, which includes a 15 kW WT simulator, a 25 kW synchronous generator and an active feedback load [30].

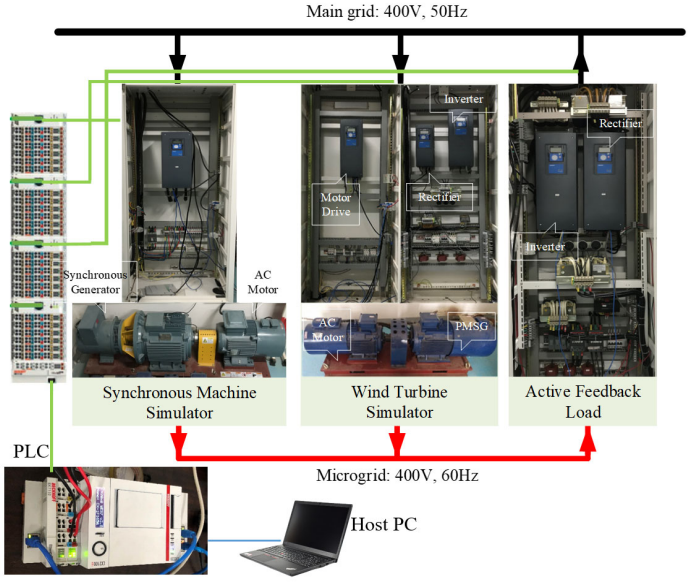

Fig. 16. Experimental tests of the proposed GDBIC scheme.

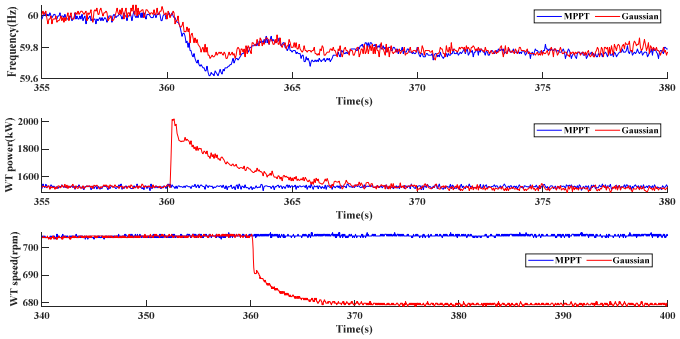

Fig. 17. The experimental results validations.

The experimental results are shown in Fig. 17. The wind speed is 6 m/s while an abrupt load change occurs from 6000 W to 7000 W at time t=360s. The WT immediately follows the proposed GDBIC method in which the frequency nadir is supported remarkably, compared with the MPPT operation mode. The rotor speed then converges to an equilibrium point as shown in the figure.

To evaluate the effects of the proposed method on the blade fatigue, the root loads and tip motions of blade are compared by applying the National Renewable Energy Laboratory's (NREL's) Fatigue, Aerodynamics, Structures, and Turbulence (FAST) code on the wind turbine simulator. Hence, Fig. 18 shows the performance of the WT during FFR operation. The statistics of blade loading and deflection are given in Table II. Blade root moment means the moment caused by the forces at the blade root, while blade tip deflection reflects the angle of deflection at the blade tip [31]. It can be observed from the Table II that the root means square (RMS) values of the edgewise and flapwise loading and bending can be alleviated by the proposed method. Therefore, when applying the proposed method, the improvement of frequency nadir is not at the cost of blade fatigue.

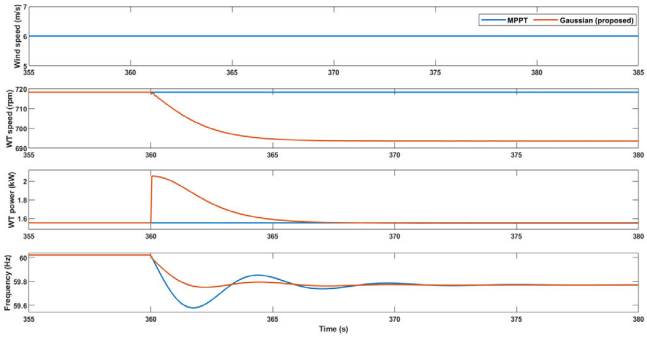

Fig. 18. The experimental results validations using FAST.

Table II Aerodynamic loading indicators on the blade with FAST

(Values in RMS)	GDBIC (proposed)	MPPT
blade root edgewise moment/(kNm)	44.5797	44.3843
blade root flapwise moment/(kNm)	2.2252	2.3206
blade tip edgewise deflection/ deg	0.0688	0.0684
blade tip flapwise deflection/ deg	0.0135	0.0139

D. Experimental Validations 2

The performance of the proposed scheme is tested using a two-area interconnected power system shown in Fig. 19(a). Details and parameters of this model are taken from [29], [32], presented in Table A.5 in the Appendix. In this case study, area 1 accommodates wind power equipped with the proposed FFR scheme. The OPAL-RT HIL testing platform is used to validate the experimental results in presence of dynamic changes in real time, as shown in Fig 19(b). It includes the RT-LAB console to model the two-area power system, send and receive signals to the real-time simulator using Modbus communication. The Analog slot board provides signals which then they are displayed by an oscilloscope in real time.

A 20% disturbance occurs in the area 1 at t=10s. The grid frequency deviation of area 1, the grid frequency deviation of area 2 and the AC tie-line power exchange are displayed in Fig. 20(a), Fig. 20(b) and Fig. 20(c), respectively. The proposed scheme achieved better frequency arrest compared with the cases of no wind farm participation and the conventional SIC scheme. As both the disturbance and wind power contribution occur in the same area 1, the frequency containment using the proposed scheme is significant.

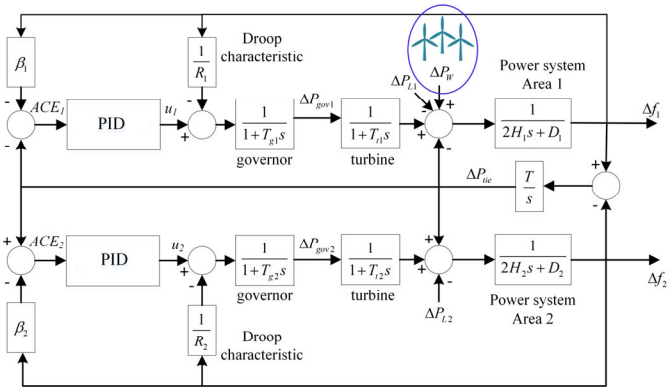

(a)

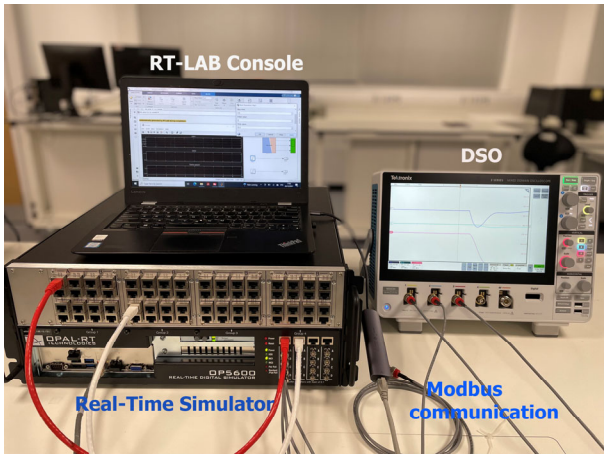

(b)

Fig. 19. The second experimental validation (a)Two-area interconnected power system in RT-LAB (b) The OPAL-RT experimental test.

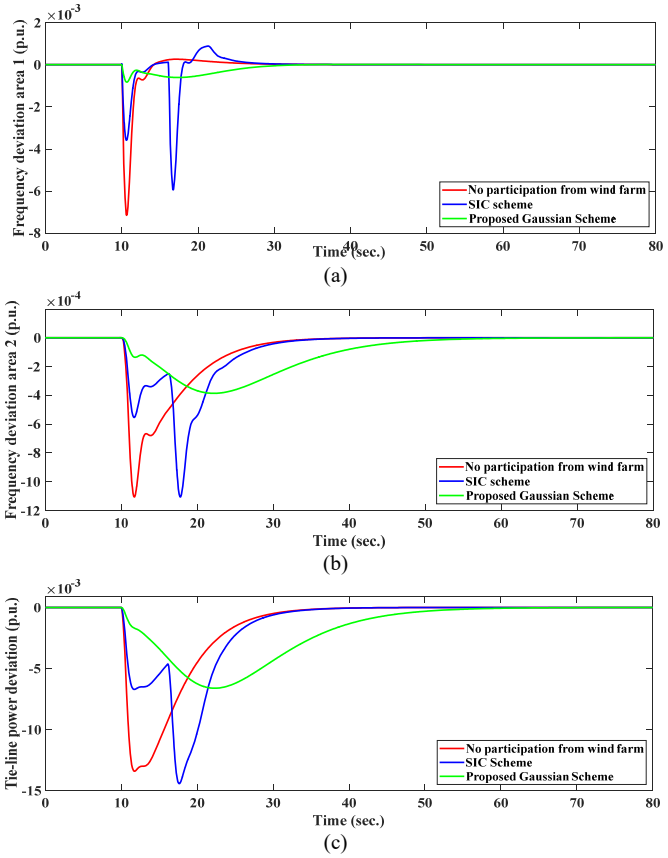

Fig. 20. Changes in the two-area frequencies and the tie-line power due to a 20% load disturbance in area 1.

When the disturbance occurs in the area 2 while the FFR comes from area 1, the frequency nadir does not improve much, as shown in Fig. 21. This indicates that a FFR scheme will contribute more to the frequency control, where the sources are located closer to the event. Therefore, it is more advantageous to provide a local control scheme where the wind turbines respond immediately to the frequency events upon receiving a command signal or by detecting the event. While this scheme is not bounded to a particular power system or region, it could directly benefit the frequency control, in line with the development of an enhanced frequency control in the Great Britain [34].

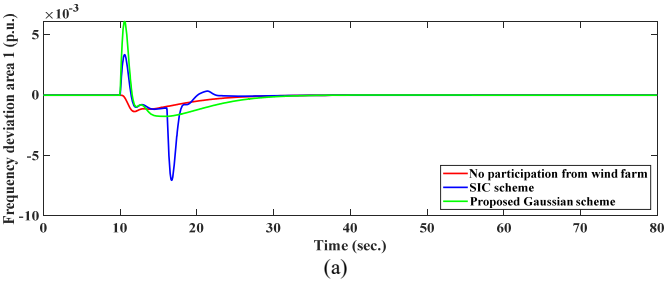

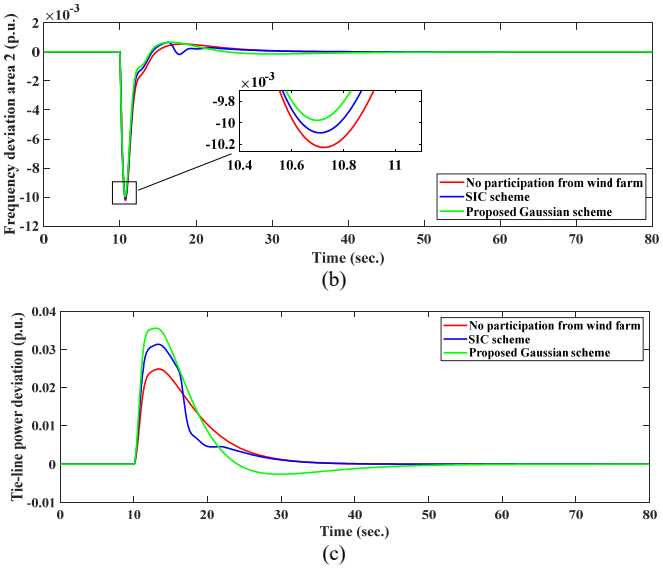

Fig. 21. Changes in the two-area frequencies and the tie-line power due to a 20% load disturbance in area 2.

V. Conclusion

The objective of this paper was to improve the grid frequency nadir using stored kinetic energy in the wind turbine (WT) rotating mass in different conditions such as wind speed change or cascade events. For this purpose, a novel Gaussian distribution-based inertial control (GDBIC) scheme was formulated and the concept that standard deviation was utilized as the control parameter was proposed. Upon detecting a power imbalance, the WTs immediately shift from the maximum power point tracking mode and inject incremental power to the grid. Then, the output power of WTs are decreased with reference to a designated Gaussian distribution trajectory with a specific standard deviation to converge to an equilibrium point. This equilibrium point has the rotor speed with the average of WT rotor speed prior to the disturbance, and the minimum mechanical stall speed limit. While the frequency nadir is improved during FFR, the settling frequency is above the maximum steady state frequency to activate AGC and bring the grid frequency back to its nominal value. In case of a cascade event during the WT's FFR, the proposed scheme will shift to another Gaussian trajectory where the new settling rotor speed will be the mean value between the rotor speed prior to the second disturbance detection, and the minimum mechanical stall speed limit. Simulations were executed on wind integrated IEEE 9-bus system and IEEE 39-bus system and comparisons with other methods were conducted. The existing methods suffer from large SFDs. Also, in presence of wind speed change, those methods are unreliable for practical implementations. However, the proposed scheme has efficiently overcome these deficiencies as well as providing highest frequency nadir improvement. The experimental tests using two different platforms were also conducted and verified the applicability and efficacy of the proposed GDBIC. In addition, the experimental tests showed that the proposed method has not increased fatigue load for the blades which is desirable for practical purposes.

In the future work, this method will be implemented on a real offshore wind turbine for grid frequency control. Also, coordination between wind turbines in a farm and among wind farms in a region can be studied to provide frequency nadir improvement considering dynamic changes of the wind speed as well as the active power change in the grid.

REFERENCES

[1] Y. Cheng, R. Azizipanah-Abarghooee, S. Azizi, L. Ding. V. Terzija, "Smart frequency control in low inertia energy systems based on frequency response techniques: A review," *Applied Energy*, vol. 279, pp. 115798, 2020.

[2] F. D´ıaz-Gonz´alez, M. Hau, A. Sumper and a. O. Gomis-Bellmunt, "Participation of wind power plants in system frequency control: Review of grid code requirements and control methods," *Renew. Sustain. Energy Rev.*, vol. 34, pp. 551–564, 2014.

[3] A. Aziz, A. T. Oo, and A. Stojcevski, "Frequency regulation capabilities in wind power plant," *Sustain. Energy Technol. Assessments*, vol. 26, pp. 47–76, 2018.

[4] J. Ekanayake and N. Jenkins, "Comparison of the response of doubly fed and fixed-speed induction generator wind turbines to changes in network frequency," *IEEE Trans. Energy Convers*., vol. 19, no. 4, pp. 800 - 802, 2004.

[5] G. Lalor, A. Mullane and M. O'Malley, "Frequency control and wind turbine technologies," *IEEE Trans. Power Syst*., vol. 20, no. 4, pp. 1905 - 1913, 2005.

[6] J. I. Yoo, Y. C. Kang, E. Muljadi, K.-H. Kim and J.-W. park, "Frequency Stability Support of a DFIG to Improve the Settling Frequency," *IEEE Access*, vol. 8, pp. 22473 - 22482, 2020.

[7] D. Yang, J. Kim, Y. C. Kang, E. Muljadi, N. Zhang, J. Hong, S.-H. Song and T. Zheng, "Temporary Frequency Support of a DFIG for High Wind Power Penetration," *IEEE Trans. Power Syst.*, vol. 33, no. 3, pp. 3428-3437, 2018.

[8] J. Morren, S. D. Haan, W. Kling and a. J. Ferreira, "Wind turbines emulating inertia and supporting primary frequency control," *IEEE Trans. Power Syst*., vol. 21, no. 1, pp. 433-434, 2006.

[9] M. Kayikci, J. V. Milanovic, "Dynamic contribution of DFIG-based wind plants to system frequency disturbances," *IEEE Trans. Power Syst.*, vol. 24, no. 2, pp. 859-867, 2009.

[10] T. Liu, W. Pan, R. Quan and a. M. Liu, "A variable droop frequency control strategy for wind farms that considers optimal rotor kinetic energy," *IEEE Access*, vol. 7, pp. 68636-68645, 2019.

[11] X. Zeng, T. Liu, S. Wang, Y. Dong and Z. Chen, "Comprehensive coordinated control strategy of PMSG-based wind turbine for providing frequency regulation services," *IEEE Access*, vol. 7, pp. 63944-63953, 2019.

[12] M. Hwang, E. Muljadi, G. Jang, and Y. C. Kang, "Disturbance-adaptive short-term frequency support of a DFIG associated with the variable gain based on the ROCOF and rotor speed," *IEEE Trans. Power Syst.*, vol. 32, no. 3, pp. 1873-1881, 2017.

[13] M. Altin, A. D. Hansen, T. K. Barlas, *et. al*., "Optimization of Short-Term Overproduction Response of Variable Speed Wind Turbines," *IEEE Trans. Sustain. Energy*, vol. 9, no. 4, pp1732-1739, 2018.

[14] Q. Jiang, *et. al.*, "Time-Sharing Frequency Coordinated Control Strategy for PMSG-Based Wind Turbine," *IEEE Journal on Emerging and Selected Topics in Circuits and Systems,* 2022, DOI: 10.1109/JETCAS.2022.3152796.

[15] W. Bao, L. Ding, Z. Liu, G. Zhu, M. Kheshti, Q. Wu and V. Terzija, "Analytically derived fixed termination time for stepwise inertial control of wind turbines—Part I: Analytical derivation," *International Journal of Electrical Power and Energy Systems*, vol. 121, pp. 1-10, 2020.

[16] Y. Guo, W. Bao, L. Ding, Z. Liu, M. Kheshti, Q. Wu and V. Terzija, "Analytically derived fixed termination time for stepwise inertial control of wind turbines—Part II: Application strategy," *International Journal of Electrical Power and Energy Systems*, vol. 121, 2020.

[17] M. Kang, K. Kim, E. Muljadi, J.-W. Park and Y. C. Kang, "Frequency control support of a doubly-fed induction generator based on the torque limit," *IEEE Trans. Power Syst.*, vol. 31, no. 6, pp. 575-4583, 2016.

[18] M. Kheshti, L. Ding, M. Nayeripour, X. Wang and V. Terzija, "Active power support of wind turbines for grid frequency events using a reliable power reference scheme," *Renewable Energy*, vol. 139, pp. 1241-1254, 2019.

[19] M. Kheshti, L. Ding, W. Bao, M. Yin, Q. Wu and V. Terzija, "Toward Intelligent Inertial Frequency Participation of Wind Farms for the Grid Frequency Control," *IEEE Trans. Ind. Informat*., vol. 16, no. 11, pp. 6772-6786, 2020.

[20] N. R. Ullah, T. Thiringer and a. D. Karlsson, "Temporary primary frequency control support by variable speed wind turbines—potential and applications," *IEEE Trans. Power Syst*, vol. 23, no. 2, pp. 601-612, 2008.

[21] M. Kang, E. Muljadi, K. Hur and a. Y. C. Kang, "Stable adaptive inertial control of a doubly-fed induction generator," *IEEE Trans. Smart Grid*, vol. 7, no. 6, p. 2971–2979, 2016.

[22] M. Kang, J. Lee and a. Y. C. Kang, "Modified stepwise inertial control using the mechanical input and electrical output curves of a doubly fed induction generator," in *Proc. 9th Int. Conf. Power Electron*., 2015.

[23] G. C. Tarnowski, P. C. Kjær, P. Sørensen and a. J. Østergaard, "Variable speed wind turbines capability for temporary over- production," in *Proc. IEEE Power Energy Soc. Gen. Meeting*, Calgary, AB, Canada, 2009.

[24] W. Bao, *et. al*., "A Hierarchical Inertial Control Scheme for Multiple Wind Farms With BESSs Based on ADMM," *IEEE Trans. Sustain. Energy*, vol. 12, no. 2, pp 1461-1472, April 2021.

[25] K. Liu, Y. Qu, H.-M. Kim, and H. Song, "Avoiding frequency second dip in power unreserved control during wind power rotational speed recovery," *IEEE Trans. Power Syst*., vol. 33, no. 3, pp. 3097–3106, May 2018.

[26] M. Toulabi, A. S. Dobakhshari, and A. M. Ranjbar, "An adaptive feedback linearization approach to inertial frequency response of wind turbines," *IEEE Trans. Sustain. Energy*, vol. 8, no. 3, pp. 916–926, Jul. 2017.

[27] M. Mehrabankhomartash, M. Saeedifard, A. Yazdani, "Adjustable Wind Farm Frequency Support Through Multi-Terminal HVDC Grids," *IEEE Trans. Sustain. Energy*, vol. 12, no. 2, pp 751-760, April 2021. DOI: 10.1109/TSTE.2021.3049762

[28] Y. Cheng, R. Azizipanah-Abarghooee, S. Azizi, *et. al.*, "Smart frequency control in low inertia energy systems based on frequency response techniques: A review," *Applied Energy*, vol. 279, pp. 115798, Dec. 2020.

[29] M. Kheshti, L. Ding, H. Askarian-Abyaneh, A. R. Singh, S. Zare and V. Terzija, "Improving frequency regulation of wind-integrated multi-area systems using LFA-fuzzy PID Control," *Int. Trans. Electr. Energ. Syst.*, vol. e12802, 2021.

[30] M. Yin, W. Li, C. Y. Chung, Z. Chen, Y. Zou, "Inertia compensation scheme of WTS considering time delay for emulating large-inertia turbines," *IET Renewable Power Generation*, vol. 11, no. 4, pp. 529-538, 2017.

[31] J. M. Jonkman and M. L. Buhl, Jr., "FAST user's guide," *National Renewable Energy Lab*., Golden, CO, USA, Tech. Rep. NREL/EL-500-38230, 2005.

[32] M. Farahani, S. Ganjefar, M. Alizadeh, "PID controller adjustment using chaotic optimization algorithm for multi-area load frequency control," *IET Control Theory Appl*., vol 6, no. 13, pp. 1984–1992, 2012. DOI: 10.1049/iet-cta.2011.0405.

[33] "Technical Report on the events of 9 August 2019," NationalgridESO, https://www.nationalgrideso.com/, 2019.

[34] "The Enhanced Frequency Control Capability (EFCC) project closing down report " NationalgridESO, https://www.nationalgrideso.com/, 2019

APPENDIX

TABLE A.1. PARAMETERS OF THE DFIG

Parameters	Units	Value
Rated Apparent Power	kVA	5556
Rated Mechanical Power	kW	4869.553
Number of Pole Pairs	-	2
Rated Voltage	kV	0.69
Nominal Speed	rpm	1485.153
Stator Resistance	p.u.	0.01
Stator Reactance	p.u.	0.1
Magnetizing Reactance	p.u.	3.5
Rotor Resistance	p.u.	0.056
Rotor Reactance	p.u.	0.031
Coefficient of MPPT control (K_{opt})	-	0.4993

TABLE A.2. TERMINAL CONDITIONS OF IEEE 9-BUS SYSTEM

Bus	V [kV]	nominal power [MW]	P [MW]	Q [Mvar]
1	16.5	247.5	50	27
2	18.0	212.5	163	10
3	13.8	170	85	0

TABLE A.3. LOAD CHARACTERISTICS OF IEEE 9-BUS SYSTEM

Bus	P [MW]	Q [Mvar]
5	125	40
6	90	30
8	100	35

TABLE A.4. TRANSMISSION LINE CHARACTERISTICS OF IEEE 9-BUS SYSTEM

Line		R [Ω/km]	X [Ω/km]
From Bus	To Bus		
4	5	5.29	44.965
4	6	8.993	48.668
5	7	16.928	85.169
6	9	20.631	89.93
7	8	4.4965	38.088
8	9	6.2951	53.3232

TABLE A.5. PARAMETERS OF THE WIND INTEGRATED TWO-AREA POWER SYSTEM

Power sys. parameter	values	Power sys. parameter	values
f	60 Hz	T	2
R_1	0.05 MW/Hz	R_2	0.0625 MW/Hz
β_1	20.6 Hz/MW	β_2	16.9 Hz/MW
T_{g1}	0.2 s	T_{g2}	0.3 s
T_{t1}	0.5 s	T_{t2}	0.6 s
H_1	5.0	H_2	4.0
D_1	0.6	D_2	0.9

Mostafa Kheshti (M'16, SM'21) received the Ph.D. degree in electrical engineering from Xi'an Jiaotong University, China, in 2017 with highest honors and scholarships. In the period 2018-2021, he was an Associate Professor at School of Electrical Engineering of Shandong University, China and the principal investigator of several funded projects. He was the recipient of Shandong University Future Young Scholars Award. He is currently a postdoctoral research fellow at the Intelligent Control and Smart Energy (ICSE) research group at School of Engineering, University of Warwick, U.K. From 2010 to 2011, he was a system operator at the Regional Dispatching Centre of Fars Regional Electric Co., Iran.
His main research interests include renewable energy integration, low inertia systems control and renewable energy-based ancillary services.

Shuyue Lin is a lecturer in electrical and electronic engineering at the University of Hull, UK. Before that, she was an assistant professor at Fuzhou University, China. She obtained her PhD in engineering (University of Warwick), MSc in control systems (Imperial College London), and BEng in electrical power engineering (the University of Bath and North China Electric Power University) in 2019, 2013, and 2012, respectively. Her current research interests include power generation and grid integration of renewable energies, fault detection and diagnosis in power systems.

Xiaowei Zhao received the Ph.D. degree in control theory from Imperial College London, London, U.K., in 2010.

He was a Post-Doctoral Researcher with the University of Oxford, Oxford, U.K., for three years before joining the University of Warwick, Coventry, U.K., in 2013. He is currently Professor of control engineering and an EPSRC Fellow with the School of Engineering, University of Warwick.

His main research areas are control theory and machine learning with applications in offshore renewable energy systems, smart grid, and autonomous systems.

Lei Ding (M'10, SM'21) received his B.E. and Ph.D. degrees in electrical engineering from Shandong University, China, in 2001 and 2007, respectively. From 2008 to 2009, he was a Postdoctoral Researcher with Tsinghua University. From 2010 to 2011, he was a Research Associate with The University of Manchester. Currently, he is the Professor at Shandong University. His research interests include low inertia system, integration of renewable energy and power system wide-area protection.

Minghui Yin (M'14) received the B.Eng. and M.Eng. degrees in electrical power engineering and the Ph.D. degree in control science and engineering from Nanjing University of Science and Technology, Nanjing, China, in 1999, 2002 and 2009, respectively. He was a research assistant with the Department of Electrical Engineering, the Hong Kong Polytechnic University, Hong Kong, from July 2007 to July 2008. He was a visiting scholar with the School of Electrical and Information Engineering, University of Sydney, Australia, from Jan. 2016 to Jan. 2017. He is currently a professor in the School of Automation, Nanjing University of Science and Technology. His major research interests include wind power conversion system and power system transient stability.

Vladimir Terzija (M'95–SM'00–F'16) was born in Donji Baraci (former Yugoslavia). He received the Dipl-Ing., M.Sc., and Ph.D. degrees in electrical engineering from the University of Belgrade, Belgrade, Serbia, in 1988, 1993, and 1997, respectively. He is a Full Professor and the Head of Laboratory of Modern Energy Systems at Skoltech, Russian Federation, where he has been since 2021. In the period 2006-2020 he was the EPSRC Chair Professor in Power System Engineering with the Department of Electrical and Electronic Engineering, The University of Manchester, Manchester, U.K. From 1997 to 1999, he was an Assistant Professor with the University of Belgrade, Belgrade, Serbia. From 2000 to 2006, he was a Senior Specialist for switchgear and distribution automation with ABB, Ratingen, Germany. His current research interests include smart grid applications, wide-area monitoring, protection and control, multi-energy systems, switchgear and transient processes, ICT, data analytics, and digital signal processing applications in power systems. Prof. Terzija is the Editor-in-Chief for the *International Journal of Electrical Power and Energy Systems*, Alexander von Humboldt Fellow, recipient of the National Friendship Award, China and Distinguished Professor with Shandong University, Jinan, China.